Tight-binding modeling of excitonic response in van der Waals stacked 2D semiconductors

Cho Tung Yip[a,†], Tsz Wing Lo[b,†], Si-Cong Zhu[b,c], Guang Yi Jia[b], Huarui Sun[a], Chi-Hang Lam[b] and Dangyuan Lei[b,*]

Atomically thin transition metal dichalcogenides (TMDCs) exhibit fascinating excitonic properties which are of critical importance for potential applications in nanoscale optoelectronics. In particular, stacked TMDC layers without lattice mismatch allow modulating their band structures and optoelectronic properties by manipulating constituent materials along the stacking direction. Current understanding of TMDC layer-by-layer structures is mainly based on optical measurements and DFT calculations. In this work, we use a phenomenological tight-binding model, combined with DFT calculations, to understand the measured layer-dependent excitonic response of WS_2. This explicit and effective model can quantitatively predict the layer-dependent excitonic states and can also be used to study interlayer excitons (direct and indirect exciton states) in TMDC multilayer structures. In addition, we find that the temperature dependence of the A exciton emission energy of monolayer WS_2 can be well described with the Varshni formula, and that the emission intensity variation with temperature is associated with thermal redistribution of exciton population and increased non-radiative damping due to the enhanced electron-phonon interation at elevated temperatures.

Introduction

Transition metal dichalcogenides (TMDCs), with a generalized formula MX_2 with M = Mo, W, or Pt, and X = S, Se, or Te, have attracted a great deal of fundamental research and technological application interests. Two-dimensional (2D) MX_2 is formed by a sandwich structure with chalcogen atoms in two hexagonal planes separated by a plane of metal atoms. Particularly, monolayer MX_2 materials exhibit direct band gaps in the visible and near-infrared region, making them ideal candidates as complementary metal oxide semiconductors. Due to the atomic thickness of 2D TMDCs, the dielectric screening effect is significantly suppressed, which is more than one order of magnitude weaker than bulk GaAs, leading to a dominant excitonic response at room temperature. The strong electron-hole interaction in these materials has triggered numerous studies in the context of many-body physics.[1-4] In addition to the influence in electronic states of many-electron systems, their optical properties have also attracted great attention. For instance, the breaking of inversion symmetry in odd-layer TMDCs enables controlling the valley polarization with circularly polarized light[5-10] and strong excitonic second-harmonic generation.[11] It has been well studied that the stacking of 2D materials with van der Waals (vdW) bond has a prominent effect on excitonic emission. A vdW heterostructure, which is deterministically formed by stacking different types of 2D materials together, can also exhibit new properties, such as long-lived interlayer excitons,[12,13] tunneling transistors, and light-emitting tunneling diodes, all absent in their constituent layers. Recently, layer-dependent ferromagnetism in a vdW CrI_3 2D material (ferromagnetism in the monolayer, anti-ferromagnetism in the bilayer, and back to ferromagnetism in the tri-layer), which is not affected by the substrate that couples with it, has been predicted[14] and observed.[15,16] Nowadays, numerical studies of exciton states with GW and Bethe–Salpeter equation (BSE) methods are regarded as a standard way to describe semiconductor excitonic effects, and their results are highly consistent with the optical measurements of various 2D materials.[17,18] Despite the success of GW and BSE in calculating the exciton states in 2D materials, an intuitive model, which can capture the essential physics of 2D layer-by-layer structures, is needed to understand the physical mechanisms of light-exciton interaction in these structures at different conditions.

In this work, we characterize the number of layers in WS_2 through examining their breathing modes in the low wavevector region, which indicates the vdW nature between WS_2 layers.[19] We then examine the layer-number-dependent *A* and *B* excitons with differential reflection spectroscopy. The extracted layer-dependent exciton resonance energies can be well described with an intuitive tight-binding model, which demonstrates a more general intepretation of the layer-dependent optical properties of WS_2 than the quantum well model with fractional-dimensional space. Finally, we observe an obvious temperature-dependent polaron effect on the photoluminescence emission energy and intensity of monolayer WS_2, consistent with the Varshni formula and the physical senario of thermal redistribution of exciton population, which reveals the similarity between the excitonic states in WS_2 and the electronic levels of traditional semiconductors.

[a.] *School of Science, Harbin Institute of Technology, Shenzhen Graduate School, Shenzhen, Guangdong 518055, China*
[b.] *Department of Applied Physics, The Hong Kong Polytechnic University, Hong Kong, China. Email: dangyuan.lei@polyu.edu.hk*
[c.] *College of Science and Key Laboratory for Ferrous Metallurgy and Resources Utilization of Ministry of Education, Wuhan University of Science and Technology, Wuhan 430065, China.*
†*Both authors contributed equally to this work*

Experimental

Synthesis. Monolayer and few-layer WS_2 triangular flakes were synthesized on 0.35 mm thick sapphire (Al_2O_3) substrates by chemical vapor deposition (CVD) reaction of WO_3 and sulfur. A sapphire wafer was first diced into 1×1 cm^2 pieces, washed in an ultrasonic bath with acetone and isopropanol, and blow dried with UHP nitrogen gas. Subsequently, WO_3 thin films were transferred into a quartz tube reactor for sulfurization for 60 min at 30 Pa and ~900 °C. A mixed Ar and H_2 flow (8:1 in volume flow rate) was used to convey WO_{3-x} vapor species to the downstream substrates, and S vapor was generated from S powders placed at the upstream of a lower temperature region (~100 °C) which was controlled independently.

Characterization. Raman spectra were recorded under excitation at 488 and 633 nm to determine the thicknesses of WS_2 flakes. Photoluminescence spectra excited at 488 and 532 nm as well as differential reflectance spectra were measured to study the thickness-dependent excitonic energies. The 532 and 633 nm lasers were equipped in a confocal optical microscope system (NT-MDT NTEGRA Spectra Solar), and the laser beams were focused on the sample surface by a 100× objective (N/A = 0.90). Optical spectra excited at 488 nm were obtained on a micro-Raman spectrometer (HORIBA HR800), and the laser beam was illuminated onto the sample through a 100× objective (N/A = 0.80). Differential reflectance is defined as $\delta R = R_W/R_S-1$, where R_W and R_S are the reflected light intensities from the sapphire substrate with and without the WS_2 flakes, respectively.[20,21] In the differential reflectance measurements, broadband white light from a tungsten quartz halogen source was focused on the sample by a 100× objective (N/A = 0.80); reflected signals were collected with the same objective and delivered to a CCD camera (Pixis 400) equipped with a spectrometer (Princeton Instrument, SP-2300) for spectral analysis.

Computational methods. Density functional theory (DFT) calculations based on conventional Kohn–Sham Hamiltonian were performed using the Perdew–Burke–Ernzerh (PBE) local density approximation (LDA).

Results and discussions

Figure 1(a) renders the optical photograph of a CVD-grown WS_2 island on a sapphire substrate, which exhibits monolayer, bilayer, multilayer, and bulk grains. The specific thicknesses (i.e., layer numbers) of this flake are determined by confocal Raman measurements. Figure 1(b) shows the corresponding Raman mapping of the A_{1g} peak intensity at 633 nm excitation, which demonstrates significant variation in Raman intensity over different grains. Low-frequency Raman spectra for points 1, 2, 3, 4, 5 and 6 as denoted in Fig. 1(a) are presented in Fig. 1(c). One traditional means to confirm the layer numbers of WS_2 is by using the high-frequency Raman modes, E^1_{2g} and A_{1g}, excited at 488 nm wavelength. Differing from the high-frequency Raman modes, low-frequency Raman spectra disclose more remarkable layer dependence, as presented in Fig. 1(c). One Raman peak at ~32 cm^{-1} can be observed from the spectrum of the bilayer grain. It undergoes a redshift as the layer number increases and appears at ~9 cm^{-1} for the six-layer region. According to the previously observed softening trend of Raman modes in MoS_2 and $MoSe_2$ with increasing layer number,[22,23] we tentatively assign this Raman peak to the layer-breathing mode, which is closely related to the number of layers of WS_2.

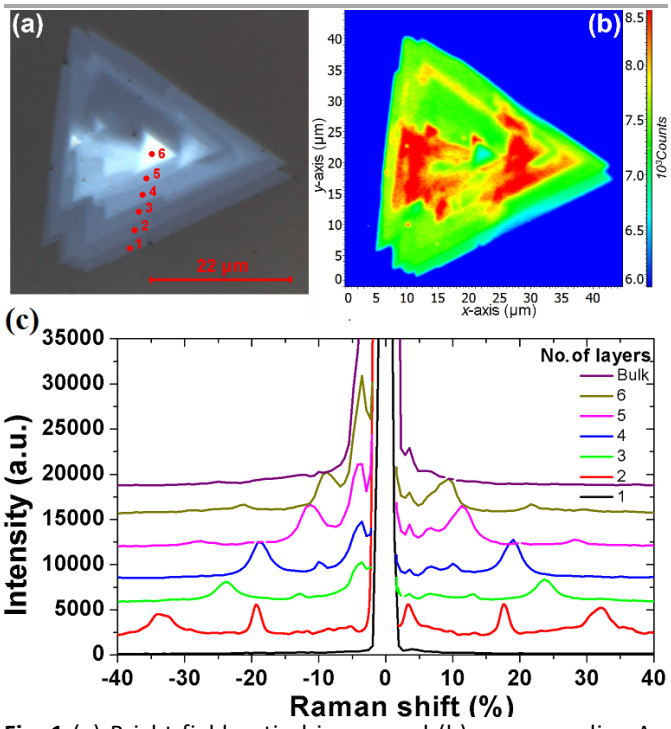

Fig. 1 (a) Bright-field optical image and (b) corresponding A_{1g} Raman intensity mapping of a WS_2 island flake; (c) Low-frequency Raman spectra of the WS_2 island measured from points 1, 2, 3, 4, 5 and 6 as denoted in (a) under 488 nm excitation, which correspond to the 1L, 2L, 3L, 4L, 5L, 6L and the bulk WS_2 regions, respectively.

Figure 2(a) shows the differential reflectance spectra of the WS_2 flake of different layer numbers. Two absorption peaks from the monolayer region can be observed at ~1.98 and ~2.36 eV, which correspond to the *A* and *B* excitonic energies, respectively. They arise from the direct gap transitions at the *K* (*K'*) points of the first Brillouin zone.[24] As the layer number increases, both *A* and *B* excitons gradually shift to lower energies. For the bulk WS_2 region, the *A* and *B* excitonic peaks shift to ~1.86 and ~2.23 eV, respectively. Figure 2(b) summarizes the peak positions of *A* and *B* excitons. It seems that the energy difference between the *A* and *B* peaks keeps approximately 400 meV for all layers, in accordance with the spin-orbit splitting energy in the valence band of WS_2.[25]

A common model used to study the layer-dependent shifts of excitonic energies in 2D TMDCs is the quantum well model with fractional-dimensional space.[26] Although this model can well fit the layer-number-dependent excitonic resonance energies with some tuning parameters, it cannot reflect the nature of vdW interlayers in which the potential energy is inhomogeneous across the structure. By making good use of the weak vdW bond between layers, we can use single-layer valance and conduction bands to span the basis of the Hamiltonian of a vdW interlayer structure. Under this condition, similar to the case of the conduction band of black phosphor vdW interlayers,[27] here we employ a phenomenological tight-binding model used for open-ended linear chain systems to model the excitonic states of TMDC vdW interlayer structures:

$$H_o = \pm\sum_{j=1}^{N}\frac{E_{go}}{2}C_j^{\dagger}C_j + \left(\sum_{j=1}^{N-1}\gamma^{(s)}\,C_{j+1}^{\dagger}C_j + h.c\right), \quad (1)$$

where E_{go} is the bandgap of the single-layer WS_2, and $\gamma^{(s)}$ is the interlayer hopping constant. As a result, the corresponding optical band gap (E_g) can be determined by the open-ended tight-binding model:

$$E_g = E_{go} - 2\left(\gamma^{(c)} + \gamma^{(v)}\right)\mathrm{Max}\left[\cos\left(\frac{n}{N+1}\pi\right)\right] \quad (2)$$

The allowed values of n are $1, 2, 3, \ldots\ldots, N$. The Hamiltonian of an exciton formed in a vdW interlayer structure is given by:

$$\left[\frac{-\hbar^2}{2\mu}\nabla^2 - \frac{e^2}{\epsilon r}\right]\varphi(r) = \left(E_{ex} - E_g\right)\varphi(r), \quad (3)$$

where $1/\mu = 1/m_h + 1/m_v$ (m_h and m_v are the effective mass of hole and electron at the valance and conduction band, respectively), $(E_{ex} - E_g) = E$ is the negative of the exciton binding energy and $E = -R/(m+\frac{1}{2})^2$ is for a 2D system, and $\varphi(r)$ is the exciton envelope function. Therefore, the corresponding transition energy of the exciton at the *K* or *K'* valley (neglecting interlayer electron-hole interaction and layer-number-dependent dielectric screening effect) can be expressed as:

$$E_{ex} = E_{go} - 2\left(\gamma^{(c)} + \gamma^{(v)}\right)\mathrm{Max}\left[\cos\left(\frac{n}{N+1}\pi\right)\right] - \frac{R_y}{\left[m+\frac{1}{2}\right]^2}, \quad (4)$$

where $\gamma^{(c)} + \gamma^{(v)} = 0.842$ eV (determined by fitting the experimental results as shown in Fig. 2(b)), and the integers m, n and N are exciton quantum number, interlayer state index and number of layers respectively, R_y is Rydberg constant for the WS_2 exciton. The layer-number-dependent characteristics in Eq. (4) is only valid for n ≥ 2 and the change in optical bandgap from n = 1 to 2 involves a direct to indirect bandgap transition (this issue will be discussed in later section).

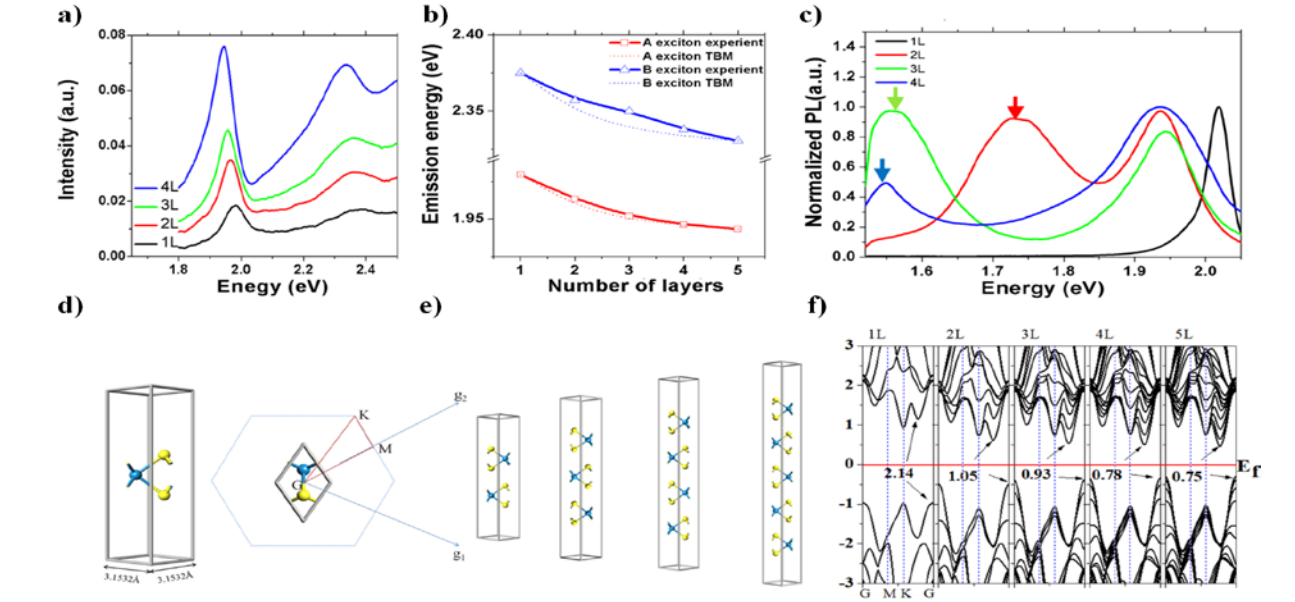

Fig. 2 (a) Differential reflectance spectra of a WS_2 island flake with different layer numbers; (b) Measured peak positions of A and B 1s state excitons with fitting curves by Eq. (3). The symbols are experimental data, and the dotted lines are the fitting results by Eq. (4); (c) Photoluminescence spectra of the same flake under 488 nm excitation; (d) and (e) are atomic structures of WS_2 for DFT calculations; (f) Calculated layer-number-dependent energy band structures, where the vertical axis is energy in eV.

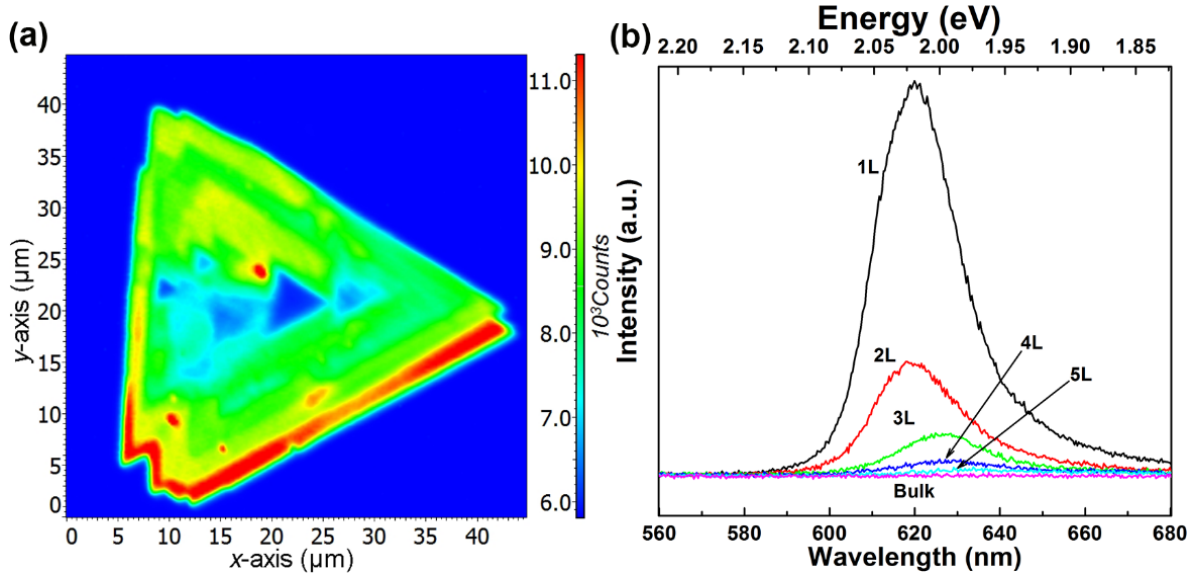

Fig. 3 (a) Fluorescence intensity map and (b) fluorescence spectra of WS_2 films with 532 nm excitation.

One can see from Eq. (4) that, the larger the layer number is, the lower the energy of excitonic transition becomes, which is in agreement with the experimental results summarized in Fig. 2(b). Due to the localization of exciton wavefunction, the ground state of the WS_2 excitons (such as A and B excitons) can be approximated as the 1s state of a 2D exciton.[17] However, an additional modification is needed to study the layer-dependent dielectric function for m > 1.[17,18] Besides the reflectance spectra, the photoluminescence spectra shown in Fig. 3(b) (for points 1, 2, 3, 4, 5 and 6 as denoted in Fig. 1(a)) also exhibit significant layer-number dependence. Figure 3(a) presents the corresponding emission intensity mapping of the WS_2 island flake at 532 nm excitation. One can see that the bulk WS_2 region shows nearly no signal, consistent with its indirect bandgap nature. As the WS_2 flake thins to a few layers, the emission intensity from direct interband transitions dramatically increases and reaches the maximum at the monolayer limit. The emission peak also shifts from ~633 nm for the 5L WS_2 to ~620 nm for the monolayer, indicating the respective direct bandgap and indirect bandgap nature of the monolayer and multilayer WS_2.[21,27-29] In theory, our DFT results show that the bandgap transits from direct to indirect when the layer number changes from monolayer to multilayer, which is different from 2D black phosphorene.[27] Therefore, the decrease in both exciton energy and optical absorption per layer from mono- to bilayer is caused by the transition from direct to indirect bandgap[21,29] rather than fractional dimension or drastic change of dielectric constant in multilayer samples.[30] The validity of the tight-binding model can be checked by ab initio GW-BSE

calculations, which explicitly include screening from the substrate and between the layers as well as self-energy and electron-hole interaction effects.[27]

The extraordinary layer-dependent electronic structure in WS_2 vdW structures is caused by the spreading of electron wavefunction between WS_2 layers.

Figure 4(a) presents the photoluminescence spectra of the monolayer WS_2 measured at different temperatures under 488 nm excitation. In order to clearly observe the shift of emission peaks, the spectra are vertically shifted from each other. Figure 4(b) shows the temperature-dependent emission peak energies extracted from Fig. 4(a), which demonstrates a continuous redshift of emission energy with increasing the temperature. Here the temperature-induced emission energy shift can be fitted with the Varshni formula:

$$E(T) = E_{go} - \alpha T^2/(T+\beta) - R_y/(m+1/2)^2, \quad (5)$$

where E_{go} is the bandgap at 0 K, α and β are phenomenological fitting parameters.[31] By using Eq. (5) to fit the emission peak positions in Fig. 4(b), we obtain E_{go} = 2.08 eV, α = 4.8×10^{-4} eV/K and β = 190 K. These parameters are comparable to that reported for excitonic emissions at low temperatures.[32] Also, one can find from Fig. 4(b) that the A exciton emission intensity reaches the maximum as the temperature increases to 353.15 K, and then gradually decreases with further increasing the temperature. The initial intensity rising may originate from the redistribution of exciton population from the underlying dark exciton states to the bright A exciton states.[1,33] Once the dark exciton redistribution saturates at fairly high temperatures, the A exciton emission may begin to suffer from larger non-radiative damping at elevated temperatures, leading to the sharp decrease in the emission intensity. In fact, both lowering of emission intensity and broadening of emission linewidth with increasing temperature are expected to be accompanied by a common effect, known as line broadening, which is due to the enhanced electron-phonon interaction at high temperatures. Nevertheless, the good agreement of the Varshni formula and the measured WS_2 excitonic emission energies illustrates an intimate connection of the excitonic response in WS_2 and the band edge tendency in traditional semiconductors. This result may originate from the shifting of band edge of WS_2 to maintain a constant binding energy as shown in Eq. (4).

Conclusions

We have examined the layer-dependent excitonic response of monolayer and vdW multilayer WS_2 through combining Raman, reflectance and photoluminescence imaging and spectroscopic measurements. We have observed a clear Raman breathing mode in the low-frequency Raman spectra of multilayer WS_2, whose Raman shift allows rapid and unambiguous identification of the number of WS_2 layers. We have used a tight-binding model, combined with DFT calculations, to semi-analytically understand the layer-dependent excitonic states in multilayer WS_2. This simple yet effective model can quantitatively predict the layer-dependent excitonic response of WS_2. We believe that the extension of this model can also be used to study interlayer excitons in general TMDC multilayer structures as well as other 2D semiconductors within the same theoretical framework. Finally, we find that the temperature-dependent emission energies of monolayer WS_2 can be well described with the Varshni formula, indicating that the temperature-induced redshift in emission energy comes from the shifting of the band edge in order to maintain a constant binding energy.

Acknowledgment

Cho Tung Yip and Huarui Sun were supported by grants from Shenzhen Municipal Science and Technology projects (Grant No. JCYJ201605313001154 and No. JCYJ20160531192714636). Tsz Wing

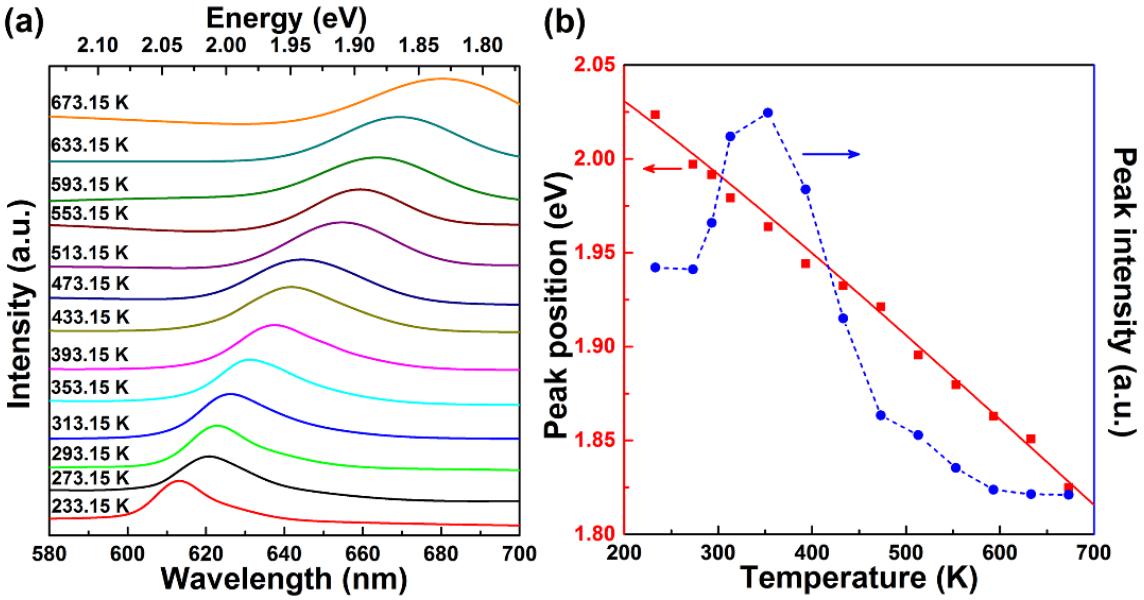

Fig. 4 (a) Temperature-dependent photoluminescence of monolayer WS_2. The spectra are vertically offset from each other for clarity. (b) Emission peak position and intensity extracted from the photoluminescence spectra in Fig. 4(a). The solid line is the fit using the Varshni formula.

Lo and Dangyuan Lei acknowledges the Hong Kong Research Grants Council (GRF grant No. 15303718).

References

1 X. X. Zhang, Y. M. You, S. Y. F. Zhao and T. F. Heinz, Phys. Rev. Lett., 2015, 115(25), 257403.
2 Z. Ye, T. Cao, K. O'Brien, H. Zhu, X. Yin, Y. Wang, S. G. Louie and X. Zhang, Nature, 2014, 513(7517), 214.
3 F. Mahmood, Z. Alpichshev, Y. H. Lee, J. Kong, and N. Gedik, Nano Lett., 2018, 18(1), 223.
4 A. Kogar, M. S. Rak, S. Vig, et al., Science 2017, 358(6368), 1315.
5 X. Di, Y. Wang, N. Qian, Phys. Rev. Lett., 2007, 99(23), 236809.
6 Y. Wang, X. Di, N. Qian, Phys. Rev. B, 2008, 77(23), 235406.
7 X. Di, G. B. Liu, W. X. Feng, et al., Phys. Rev. Lett., 2012, 108(19), 196802.
8 K. F. Mak, K. L. He, J. Shan, et al., Nat. Nanotech., 2012,7(8), 494.
9 T. Cao, G. Wang, W. P. Han, et al., Nat. Commun., 2012, 3, 887.
10 H. L. Zeng, J. F. Dai, Y. Wang, et al., Nat. Nanotech., 2012, 7(8), 490-493.
11 G. Wang, X. Marie, I. Gerber, et al., Phys. Rev. Lett., 2015, 114(9), 097403.
12 P. Rivera, K. L. Seyler, H. Y. Yu, et al., Science, 2016, 351(6274), 688-691.
13 P. Rivera, J. R. Schaibley, A. M. Jones, et al., Nat. Commun., 2015, 6, 6242.
14 W.B. Zhang, Q. Qu, P. Zhu, C.H. Lam, J. Mat. Chem. C, 3(2015), 12457.
15 B. Huang, G. Clark, E. Navarro-Moratalla, et al., Nature, 2017, 546(7657), 270.
16 C. Gong, L. Li, Z. L. Li, et al. Nature, 2017, 46(7657), 265.
17 D. Y. Qiu,F.H.da Jornada, S. G. Louie, Phys. Rev. Lett., 2013, 111(21), 216805.
18 D. Y. Qiu, F. H. da Jornada, S.G. Louie, Phys. Rev. B, 2016, 93 (23), 235435.
19 Y. Y. Zhao, et al. Nano Lett., 2013, 13(3), 1007.
20 K. F. Mak, et al. Phys. Rev. Lett., 2008, 101(19), 196405.
21 K. F. Mak, C. G. Lee, J. Hone, et al., Phys. Rev. Lett., 2010, 105(13), 136805.
22 M. O'Brien, N. McEvoy, D. Hanlon, et al. Sci. Rep., 2016, 6, 19476
23 A. A. Puretzky, L. B. Liang, X. F. Li, et al. ACS Nano, 2015, 9(6), 6333.
24 D. C. Kozawa, R. Kumar, A. Carvalho, et al. Nat. Commun., 2014, 5, 4543.
25 W. J. Zhao, Z. Ghorannevis, L. Q. Chu, et al. ACS Nano, 2013,7 (1),791-797.
26 Y. L. Yu, Y. F. Yu, Y. Q. Cai, et al. Sci. Rep., 2015, 5, 16996.
27 L. K. Li, J. Kim, C. H. Jin, et al., Nat. Nanotech.,2017, 12(1), 21-25.
28 B. R. Zhu, X. Chen, X. D. Cui, Sci. Rep., 2015, 5, 9218.
29 H. L. Zeng, G. B. Liu, J. F. Dai, et al., Sci. Rep., 2013, 3, 1608.
30 G. Y. Jia, Y. Liu, J. Y. Gong, D. Y. Lei, D. L. Wang, Z. X. Huang, J. Mater. Chem. C, 2016, 4, 8822-8828.
31 D. W. Snoke, Solid State Physics Essential Concepts, PearsonAddison-Wesley, 2009.
32 D. Stich, J. Zhou, T. Korn, et al., Phys. Rev. Lett., 2007, 98 (17), 176401.
33 T. W. Lo, Q. Zhang, M. Qiu, et al., "Thermal redistribution of exciton population in monolayer transition metal dichalcogenides probed with plasmon-exciton coupling spectroscopy", 2019, under review.